International Journal of Nanomedicine

Dovepress
open access to scientific and medical research

Open Access Full Text Article

ORIGINAL RESEARCH

Evaluation of the Ocular Safety of Hollow Mesoporous Organosilica Nanoparticles with Different Tetrasulfur Bond Content

Juan Li[1,*], Ziqing Gao[1,*], Ning Li[1], Ling Yao[1], Chao Liu[1], Che Xu[1], Xiaohui Ren[1], Aiqin Wang[1], Siqi Gao[2], Miao Wang[2], Xiang Gao[2], Kun Li[3], Jianfeng Wang[1]

[1]Department of Ophthalmology, First Affiliated Hospital of Bengbu Medical University, Bengbu, Anhui, 233004, People's Republic of China; [2]School of Clinical Medicine, Bengbu Medical University, Bengbu, Anhui, 233004, People's Republic of China; [3]School of Life and Health Science, Anhui Science and Technology University, Fengyang, Anhui, 233100, People's Republic of China

*These authors contributed equally to this work

Correspondence: Kun Li; Jianfeng Wang, Email liangliang2419@126.com; wangjianfeng1969@163.com

Background: Drug therapy for eye diseases has been limited by multiple protective mechanisms of the eye, which can be improved using well-designed drug delivery systems. Mesoporous silica nanoparticles (MSNs) had been used in many studies as carriers of therapeutic agents for ocular diseases treatment. However, no studies have focused on ocular biosafety. Considering that MSNs containing tetrasulfur bonds have unique advantages and have drawn increasing attention in drug delivery systems, it is necessary to explore the ocular biosafety of tetrasulfur bonds before their widespread application as ophthalmic drug carriers.

Methods: In this study, hollow mesoporous silica nanoparticles (HMSNs) with different tetrasulfur bond contents were prepared and characterized. The ocular biosafety of HMSN-E was evaluated in vitro on the three selected ocular cell lines, including corneal epithelial cells, lens epithelial cells and retinal endothelial cells (HREC), and in vivo by using topical eye drops and intravitreal injections.

Results: In cellular experiments, HMSNs caused obvious S content-dependent cytotoxic effect. HMSNs with the highest tetrasulfur bond content (HMSN-E), showed the highest cytotoxicity among all the HMSNs, and HREC was the most vulnerable cell to HMSN-E. It was shown that HMSN-E could react with intracellular GSH to generate H_2S and decrease intracellular GSH concentration. Treatment of HREC with HMSN-E increased intracellular ROS, decreased mitochondrial membrane potential, and induced cell cycle arrest at the G1/S checkpoint, finally caused apoptosis and necrosis of HREC. Topical eye drops of HMSN-E could cause corneal damage. The intravitreal injection of HMSN-E could induce inflammation in the vitreum and ganglion cell layers, resulting in vitreous opacities and retinal abnormalities.

Conclusion: The incorporation of tetrasulfur bonds into HMSN can have toxic effects on ocular tissues. Therefore, when mesoporous silica nanocarriers are designed for ophthalmic pharmaceuticals, the ocular toxicity of the tetrasulfur bonds should be considered.

Keywords: ophthalmic safety, hollow mesoporous silica nanoparticles, ophthalmic drug delivery, tetrasulfur bond

Introduction

The eye is a highly complex, isolated, and sophisticated sensory organ of the human body. Anatomically, there are multiple protective mechanisms in the eye, such as the ear, turnover, reflex blinking, and nasolacrimal drainage.[1–3] However, vision is still easily impaired in various diseases.[4–7] Although drug therapy is the main treatment for most eye diseases, the multiple protective mechanisms of the eye pose a significant limitation for therapeutic drugs to reach the intended site and maintain an effective drug concentration.[8,9] Fortunately, the development of nanotechnology has resulted in significant progress and breakthroughs in ocular drug delivery.[9–20] Nano-drug delivery systems have various advantages, such as sustained and controlled drug release, enhanced transcorneal permeability, long drug residence time, and drug targeting, which may reduce dosing frequency and improve patient compliance.[21,22] Although many drug

Received: 18 February 2024
Accepted: 27 June 2024
Published: 16 July 2024

nanocarriers have been investigated for the treatment of anterior and posterior ocular diseases and display differential advantages, they also face many limitations, such as instability of the carrier system, low loading capacity, and high cost.[23–25]

Mesoporous silica nanoparticles (MSNs) have become promising nanosystems because of their unique properties in drug delivery systems, such as 1) large pore volume and high surface area, 2) high loading capacity, 3) adjustable morphology, 4) easily modifiable surface, 5) good biocompatibility and biodegradability, and 6) high stability under physiological conditions. Various MSN-based nanosystems had been designed as carriers of therapeutic agents, including small drug molecules, proteins, and nucleic acids, to treat various diseases, including ocular diseases.[26–31] For example, carboplatin, pilocarpine, topotecan, sodium nitroprusside, and bevacizumab have been encapsulated into MSNs for the treatment of ocular diseases.[32–37] Although MSNs have gained increasing interest in ocular drug delivery systems, limited ocular biosafety research poses potential concerns for their clinical application.[30–32,37] Silica is "generally recognized as safe" by the Food and Drug Administration (FDA) and is currently used as an excipient in some medications. Recently, silica nanoparticles have been approved by the FDA for cancer treatment in several clinical trials for treating cancer.[38,39] Many studies have shown that silica nanoparticles can undergo rapid degradation under physiological conditions to generate non-toxic silicates, and their biosafety has been proven to be safe within an appropriate dosage range.[39–43] The incorporation of disulfide or tetrasulfur bonds into the structure of MSNs can endow carriers with GSH-responsive degradability.[44–53] In addition, the biosafety and biocompatibility of MSNs in vivo have been evaluated via various routes of administration, including intravenous, oral gavage, and intraperitoneal administration.[41] However, no studies have focused on the influence of MSNs on ocular tissues. Anatomically, the eye is an isolated and specialized organ in human body as compared with other organs, which necessitates the evaluation of ocular safety of MSNs. Among MSNs, hollow mesoporous silica nanoparticles (HMSNs) possess an internal hollow structure that can provide greater encapsulation capacity than other MSNs and a controllable shell structure that can endow the carriers with a more flexible functional design. HMSNs have always been a focus in drug delivery system.[54–56] Therefore, this study focused on the ocular biosafety of HMSNs.

Recently, many drug delivery systems that can generate hydrogen sulfide (H_2S) have been developed to achieve synergistic effects with other therapeutic modalities.[57–59] It was reported that the incorporation of tetrasulfur bonds into MSNs could not only endow the carriers with GSH-responsive degradability but also form a GSH-induced H_2S nanogenerator, which could lead to cytotoxicity on tumor cells. H_2S is a gasotransmitter that regulates several pathophysiological processes.[60,61] High H_2S concentrations can induce tumor cell death via various mechanisms,[62,63] suggesting that high H_2S concentrations might exert potential toxicity on normal tissue cells. Therefore, in this study, HMSNs with different tetrasulfur bond contents were prepared and characterized. The effects of HMSNs on three types of ocular cells were investigated to evaluate the potential toxic effects of HMSNs. Finally, the effect of HMSNs on mouse eyes was evaluated using intravitreal injections and topical eye drops. This study provides a significant biosafety reference for the application of HMSNs in ophthalmology.

Materials and Methods

Materials

Glutathione (reduced, 98%), MTT (≥98.0%), Na_2CO_3 (≥99.5%), DMSO (≥99.9%), anhydrous ethanol (99.5%), tetraethyl orthosilicate (TEOS, 98%), bis[3-(triethoxysilyl)propyl] tetrasulfide (BTESPT, 90%), triethylamine (99%), cetyltrimethylammonium bromide (CTAB) (99%), 5,5′-dithiobis(2-nitrobenzoic acid) (DTNB, 98%), and aqueous ammonia (AR, 25–28%) were purchased from Shanghai Aladdin Biochemical Technology Co., Ltd. Washington State Probe-1 (WSP-1, H_2S probe) was purchased from MKBio (Shanghai, China). Fetal bovine serum (FBS) was purchased from Shanghai Zhongqiao Xinzhou Biotechnology Co. Ltd. Trypsin and all KITs used in this study were purchased from Shanghai Biyuntian Biotechnology Co. Ltd. The TNF-α Immunohistochemical reagent kit was purchased from Sangon Biotech Co. Ltd.(Shanghai, China). All other chemicals and solvents used were of analytical grade.

Cell Culture

Human corneal epithelial cells (HCE-T), lens epithelial cells (HLEC) and retinal endothelial cells (HREC) were purchased from the ATCC. The cells were cultured in DMEM supplemented with 10% FBS and 100 U/mL penicillin.

Methods

Synthesis of HMSNs

HMSNs were prepared based on the Stöber method with some modification.[64,65] To prepare Stöber-based silica nanoparticles as the hard template, 60 mL anhydrous ethanol, 5 mL ddH_2O and 2 mL ammonia water were mixed by magnetic stirring for 10 min in a PTFE Beaker. Subsequently, 2.4 mL TEOS was added and the reaction lasted for 2 h under continuous magnetic stirring. The silica nanoparticles were collected by centrifugation (12000 rpm for 10 min) and resuspended in 100 mL of ddH_2O. Subsequently, 5 g of CTAB and 0.5 mL triethanolamine solution (0.2 mg/mL) were added and dissolved under continuous magnetic stirring at 80 °C. And then 1.44 mL mixture of TEOS and BTESPT was added, and the reaction was continued for 6 h under continuous magnetic stirring at 80 °C. After the reaction was complete, the organic-inorganic hybrid silica was collected by centrifugation (12000 rpm for 10 min) and subsequently resuspended in 200 mL of ddH_2O. The suspension was magnetically stirred at 60 °C for 60 min. Subsequently, 8 g Na_2CO_3 was added to the suspension and allowed to react for 60 min. Finally, HMSNs were obtained by centrifugation (12000 rpm for 10 min). The etched HMSNs were washed with DI water and then were resuspended in 500 mL of an HCl/ethanol solution (10:90, v/v) to remove CTAB. HMSNs with different S contents were prepared by adjusting the volume ratio of BTESPT in the 1.44 mL mixture of TEOS and BTESPT (0% for HMSN-A, 25% for HMSN-B, 50% for HMSN-C, 75% for HMSN-D and 100% for HMSN-E, respectively).

Characterization of HMSNs

The morphologies and hollow mesoporous structures of the samples were determined using scanning electron microscopy (SEM, JEOL, Kyoto, Japan, JSM7800F) and TEM (JEOL, Kyoto, Japan, 2100F, 200KV). The specific surface area and pore size distribution were determined using linear regression with the BET model and the Barrett–Joyner–Halenda (BJH) method via specific surface area and porosity analyzer (Micromeritics, USA, ASAP2460). The S content of the HMSNs was analyzed using an organic element analyzer (Elementar, Vario EL Cube).

H_2S-Generation from the Reaction of HMSNs with GSH

In the in vitro studies, 5 mg of HMSNs were suspended in 1.5 mL of buffer solution (pH 4) containing 10 mM GSH in 2 mL of EP. After ultrasonic mixing, pieces of lead nitrate test strips were cut off to cover the EP openings, and scotch tape was used to fix the test strip onto the EP openings. At the determined time, pieces of the lead nitrate test strip were carefully uncovered. The blackness was analyzed using a handheld colorimeter (LS171, Shenzhen Linshang Technology Co., Ltd). Washington State Probe-1 (WSP-1, H_2S probe) was used to detect the intracellular generation of H_2S in HREC. HREC (5×10^4 cells per well) were first seeded into 6-well culture plates and then cultured for 18 h. Next, the medium was discarded, and the cells were washed once with PBS. The cells were stained with 0.05 mL WSP-1(25 μM) for 30 min, followed by the addition of 0.15 mL new cell culture medium containing HMSN-E. After incubation for 24 h, the cells were washed with PBS for 3 times, and detached by trypsinization. Cells were collected by centrifugation and washed twice with PBS. Finally, the green fluorescence of approximately20000cells was measured by flow cytometry.

The Cytotoxicity of HMSN Evaluated by MTT Assay

Three different types of cell lines in ocular tissues, HCE-T, HLEC, and HREC, were selected to evaluate the biosafety of HMSNs at the cellular level. Briefly, cells were seeded in 96-well plates (8×10^3 cells/well). After 24 h of incubation, the cells were treated with culture medium containing HMSNs. After further incubation for 48 h, 50 μL of MTT solution (1 mg/mL) was added to each well, and the cells were incubated for 4 h. After carefully removing the supernatant, DMSO (150 μL) was added to each well. The plates were shaken on a shaking table for 30 min. Finally, the OD_{540nm} of each well was measured using a microplate reader (Multiskan GO, Thermo Scientific, USA).

The Depletion of GSH by HMSNs

HMSNs (5 mg) was resuspended in 1.5 mL of 10 mM GSH solution (pH =4) to react for 24 h. After the solutions were centrifuged (12000 rpm for 10 min), 0.05 mL supernatant was collected using a pipette and added to 2 mL EP. And then, 1.4 mL $NaHCO_3$ (0.1M) and 0.1mL DTNB (10 mM) were subsequently added to the EP and immediately sealed. After shaking for 30 min, the absorbance of each solution was measured at 412 nm. The absorption of the control group without HMSNs was set at OD_0. The absorption of the other groups was set as OD_x. The GSH depletion rate (%) was calculated as follows:

$$\text{The depletion rate of GSH}\,(\%) = (OD_0 - OD_x) * 100\% / OD_x$$

Apoptosis and Necrosis of Cells

An Annexin V-FITC apoptosis detection kit (Beyotime, China) was used to analyze cell apoptosis and necrosis. HREC were seeded into 6-well plates (5×10^4 cells/well) and incubated for 18 h. The cells were treated with 2.5 mL fresh culture medium containing HMSN-E. After incubation for 24 h, the cells were washed with PBS for 3 times, and detached by trypsinization. Cells were collected by centrifugation and washed twice with PBS. Finally, the cells were double stained with Annexin V and propidium iodide (PI). Finally, the prepared cells (approximately20000cells) were collected and analyzed using flow cytometry.

Cell Cycle Distribution

The Cell Cycle and Apoptosis Analysis Kit (Beyotime, China) was used to investigate cell cycle distribution. Briefly, HREC were seeded in 6-well plates (5×10^4 cells/well) and incubated for 18 h. The cells were then treated with 2.5 mL fresh culture medium containing HMSN-E and incubated for another 24 h. The cells were detached by trypsinization and washed twice with PBS. After being collected by centrifugation and washed once with PBS, the cells were treated according to the manufacturer's instructions. The prepared cells (approximately20000cells) were collected and analyzed using flow cytometry.

Intracellular ROS Assay

A ROS Assay Kit (Beyotime, China) was used to detect changes in intracellular ROS levels. HREC were seeded into 6-well plates (5×10^4 cells/well) and incubated for 18 h. The cells were then treated with 2.5 mL fresh culture medium containing HMSN-E and incubated for another 24 h. The cells were detached by trypsinization, washed twice with PBS, and resuspended in serum-free medium containing 10 μmol/L DCF-DA. After incubation for 20 min in an incubator, DCF fluorescence intensity was detected using flow cytometry at an excitation wavelength of 488 nm and an emission wavelength of 525 nm.

Detection of MMP

Changes of cellular mitochondrial membrane potential (MMP) were investigated by flow cytometry using an MMP assay kit with the JC-1 dye (Beyotime, China). HREC were seeded in a 6-well plate (5×10^4 cells/well) and incubated for 18 h. The cells were treated with 2.5 mL fresh culture medium containing HMSN-E and incubated for another 24 h. The cells were detached by trypsinization, washed twice with PBS, collected by centrifugation, and stained with JC-1 according to the manufacturer's instructions. Finally, the prepared cells (approximately20000cells) were collected and analyzed using flow cytometry.

The Ocular Biosafety of HMSN in vivo

Female mice (6–8 weeks old) were randomly divided into four groups for topical eye drop administration (n=3), and five groups for intravitreal injection (n=3). All the animals had free access to food and water. For topical eye drops, 0.1 mL HMSN-E (50, 100, and 200 μg/mL) suspended in PBS was applied to one eye. PBS was used as a control. Eye drops were administered four times daily for 2 weeks. For intravitreal injections, 50 μL HMSN-E (5, 10, and 20 μg/mL) was injected into the vitreous. The PBS group was injected with 50 μL of PBS, and the control group was not injected. The mice were anesthetized after one week. For topical eye drops, pictures of mouse eyes were recorded using a slit-lamp microscope after staining the cornea with fluorescein. For intravitreal injections, pictures of the mouse eyes were recorded using a slit-lamp microscope. The eyeballs were carefully removed using surgical forceps and scalpels, washed with PBS, and fixed in 4% polyformaldehyde at 4 °C for 3 days. The fixed eyeballs were immersed into a gradient concentration of alcohol for dehydration and then processed for paraffin sectioning and routine histology with

hematoxylin and eosin (HE) staining and immunohistochemical staining. The tissues were microscopically observed using a microscopy imaging system (AxioScope.A1, Oberkochen, Germany).

Results and Discussion

Synthesis and Characterization of HMSNs

In this study, Stöber-based silica nanoparticles were prepared as hard templates by hydrolysis and condensation of silicon alkoxides. Silica nanoparticle cores were coated with mesoporous organic-inorganic hybrid organosilica by hydrolysis and condensation of a mixture of TOES and BTESPT with CTAB as a directing agent. The silica cores were selectively removed using Na_2CO_3 at 80 °C to obtain the HMSNs.

The change of volume ratio of BTESPT to TEOS can lead to different tetrasulfur bond contents in the HMSNs, which can be observed from the S content in the HMSN (Table 1). HMSN-D and HMSNN-E, with high S content (13.947% and 15.58%, respectively), displayed irregular spherical shapes (Figure 1). In previous studies, various organosilica precursors were used to incorporate organic groups into the shell of HMSNs to increase the degradation of HMSNs. Excessive organic groups in the HMNSs could increase the flexibility of the shell layer and affect its morphology.[66–68] In this study, the excessive incorporation of tetrasulfur bonds deformed the HMSNs into a bowl-like shape, similar to previously reported deformable hollow periodic mesoporous organosilica nanocapsules.[66]

Table 1 shows that the BET surface area and pore volume initially increased and then decreased with increasing S content. HMSN-C had the highest values. It has been reported that the embedment of organic groups in HMNSs could result in the expansion of the shell layer, which might lead to an increase in the BET surface area and pore volume. However, the deformation of the round morphology into an irregular bowl-like morphology could result in a decrease in the BET surface area and pore volumes.[66–68] In this study, the HMSNs remained spherical when the S content was increased from 0 to 10.873%. Therefore, the increased S content resulted in increased BET surface area and pore volume. When the S content reached 13.947% and 15.58%, the deformed bowl-like shape reduced the BET surface area and pore volume, respectively. However, the deformed bowl-like shape did not influence their capacity to load drug molecules because HMSNs with a flexible shell layer might recover their spherical shape when dispersed in organic or aqueous solvents.[67] In contrast, the average pore size increased with increasing S content. As the organosilica precursor content increased, the length of the organic chains (-Si-C-C-C-S-S-S-S-C-C-C-Si-) in the silica shells increased, which might have increased the average mesoporous pore size. Moreover, the hydrophobic organosilica precursors might serve as an oil phase to enter the CTAB micelles and enlarge them, leading to an increase in the average mesoporous pore size.

The Reaction of HMSN with GSH

Tetrasulfur bonds incorporated into MSNs could endow MSNs with GSH-responsive degradability.[44–53] In this study, DTNB was used to detect the reaction between tetrasulfur bonds and GSH in vitro. As shown in Figure 2A, when HMSNs with different S contents were incubated with GSH for 36 h, GSH depletion increased when the S content in the HMSNs increased. It could be inferred that the tetrasulfur bond in the HMSNs reacted with GSH.

Results from the lead acetate test strip assay showed that HMSNs containing tetrasulfur bonds could lead to the test strip turning black (Figure 2B and C), which indicated that the reaction of the tetrasulfur bond with GSH resulted in the generation of H_2S. A colorimeter device was used to detect the black intensity of test strip, which showed that the black

Table 1 The Content of S, Surface Area, Pore Volume and Average Pore Size

	S Contents	BET Surface Area (m^2/g)	BET Pore Volume(cm^3/g)	Average Pore Size
HMSN-A	0	423.3994	0.456370	5.0243
HMSN-B	6.616%	546.3719	0.809568	8.6141
HMSN-C	10.873%	567.3634	0.980262	8.5560
HMSN-D	13.947%	384.5626	0.875331	9.4963
HMSN-E	15.58%	388.3738	0.951507	10.5556

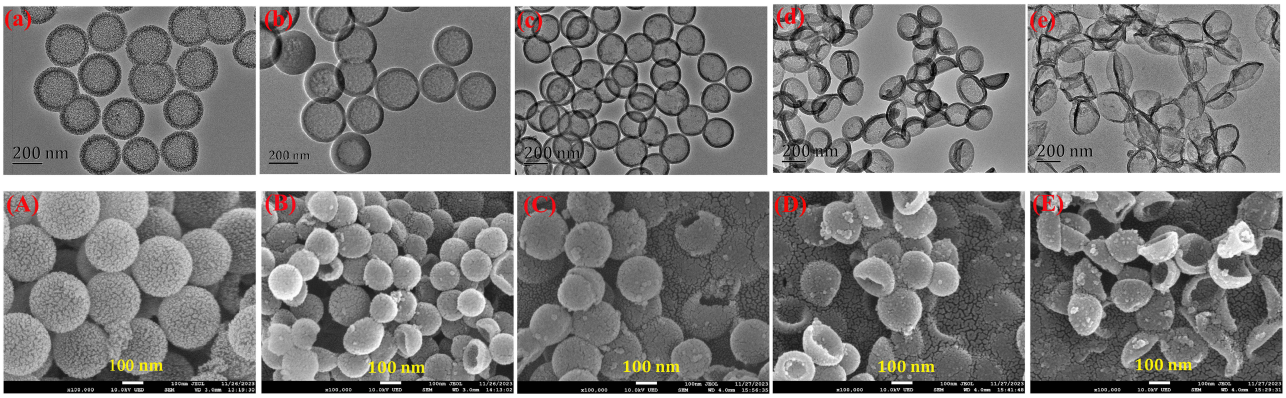

Figure 1 The images of TEM and SEM for HMSNs. (**a**–**e**) TEM for HMSN-A (**a**), HMSN-B (**b**), HMSN-C (**c**), HMSN-D (**d**) and HMSN-E (**e**), respectively (Scale bar = 200 nm). (**A**–**E**) SEM for HMSN-A (**A**), HMSN-B (**B**), HMSN-C (**C**), HMSN-D (**D**) and HMSN-E (**E**), respectively (Scale bar = 100 nm).

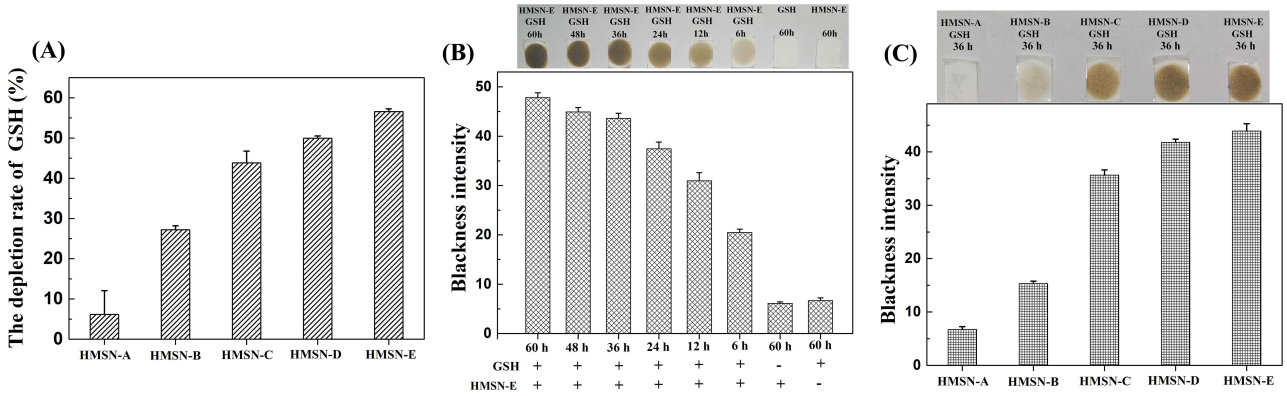

Figure 2 The reaction of GSH with HMSN in vitro. (**A**) the depletion of GSH detected by Ellman agents. (**B**) H_2S-generation detected by lead nitrate test strip from the reaction of GSH with HMSN-E for different times. (**C**) H_2S-generation detected by lead nitrate test strip from the reaction of GSH with HMSNs containing different tetrasulfide groups.

intensity increased with the elevation of the S content and the reaction time of HMSN-E with GSH. Therefore, the generation of H_2S is a tetrasulfur content- and reaction-time dependent process.

The Cytotoxicity of HMSN by MTT Assay

The MTT assay showed that HMSN-E exerted a dose-dependent inhibitory effect on the survival rate of the three cell lines and exerted a maximum toxic effect on HREC (Figure 3A). When the HMSNs contents were fixed at 200 μg/mL, the cytotoxicity of the HMSNs was positively correlated with S content (Figure 3B). HMSN-A without tetrasulfur bonds showed almost no toxicity toward HREC. It can be inferred that the tetrasulfur bonds might be involved in the toxic effect of HMSNs on HREC. In subsequent studies, HREC (the most vulnerable cells) and HMSN-E (with the highest tetrasulfur content) were selected to investigate the toxic mechanism of HMSN containing tetrasulfide.

The Mechanism for the HMSN-E Induced Cytotoxicity

The intracellular GSH content is ~100–1000 times more than the extracellular GSH content.[69] MSNs with tetrasulfur bonds were prepared to serve as a H_2S-generator nanocarriers for tumor treatment. Tetrasulfur bonds can react with GSH to result in the degradation of HMSNs and the consumption of intracellular GSH and simultaneously release H_2S, which can induce cell apoptosis at high concentration.[60,61] In this study, it was proved that HMSN-E could react with GSH to generate H_2S in vitro. Herein, a WSP-1 (H_2S probe) was used to detect intracellular generation of H_2S in HREC. As shown in Figure 4A and B, after incubation with different concentrations of HMSN-E, HREC exhibited a stronger green

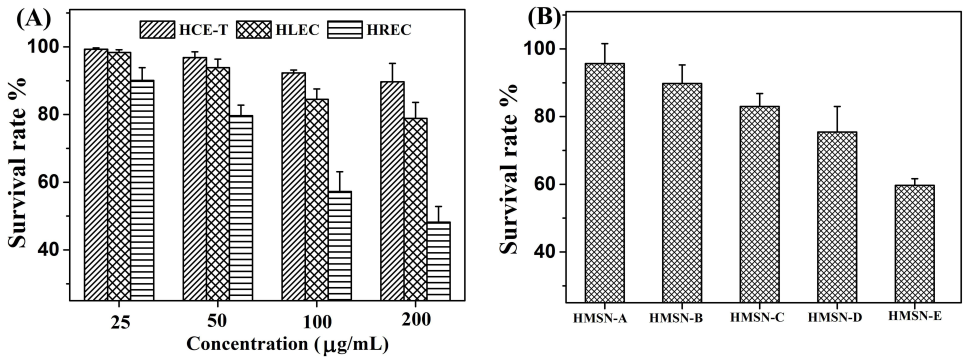

Figure 3 The effect of HMSNs on the survival rate of selected cell lines. (**A**) The survival rate of HCE-T, HLEC and HREC incubated with different concentrations of HMSN-E for 48 h, measured by MTT assay (All samples were run in triplicate). (**B**) The survival rate of HREC incubated with 0.2 mg/mL HMSNs with different S concentrations for 48 h, measured by MTT assay (All samples were run in triplicate).

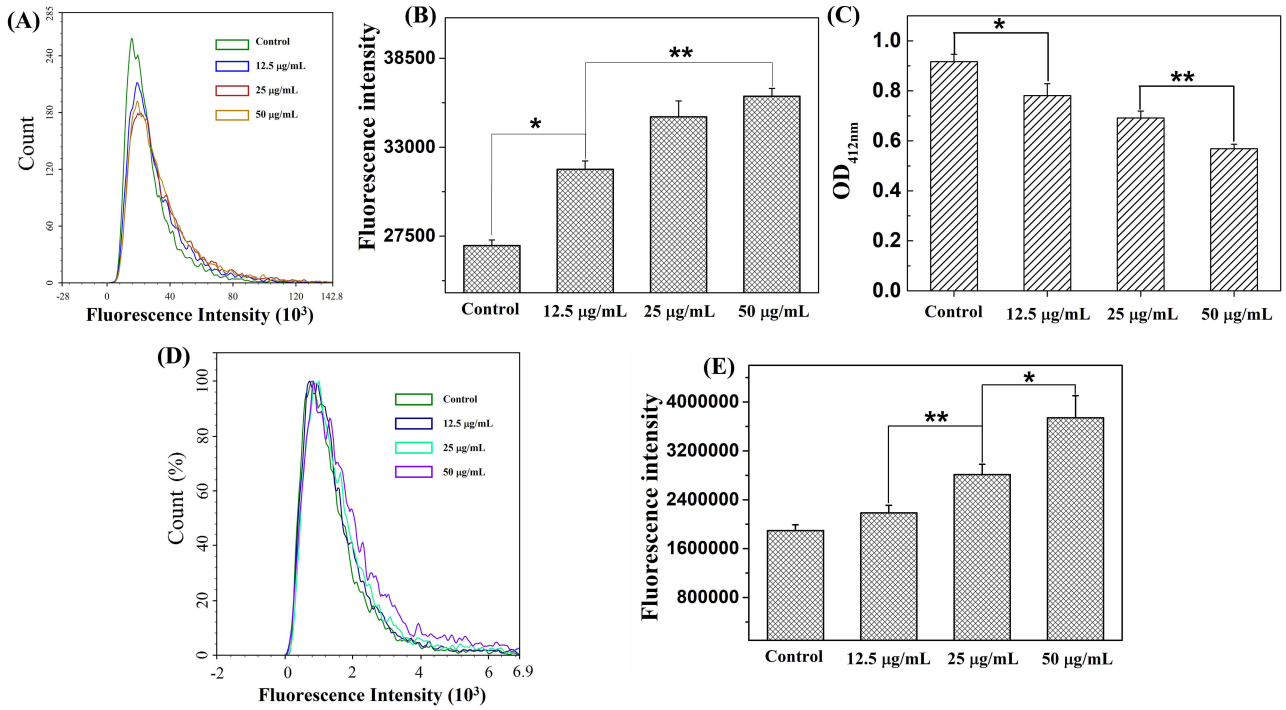

Figure 4 The effect of HMSN-E on the cellular GSH and ROS. (**A**) Flow cytometric analysis of HREC stained with WSP-1 and treated by HMSN-E. (**B**) fluorescence intensity for WSP-1 in HREC treated by HMSN-E analyzed flow cytometric analysis. (**C**) the influence of HMSN-E on intracellular GSH analyzed by DTNB method. (**D**) intracellular ROS in HREC treated by HMSN-E analyzed flow cytometric analysis.(**E**) fluorescence intensity for DCF in HREC treated by HMSN-E analyzed flow cytometric analysis. (*P*-values < 0.05 were considered statistically significant, denoted as **P* < 0.05; ***P* < 0.01).

fluorescence than the control group. The fluorescence intensity increased with increasing HMSN-E concentration, indicating that HMSN-E could induce the generation of H_2S in HREC.

The reaction of tetrasulfur groups with GSH could result in the consumption of intracellular GSH, which might disrupt the intricate redox balance in cells and cause an increase in intracellular ROS.[70] As shown in Figure 4C, intracellular GSH levels decreased as the concentration of HMSN-E increased, indicating that HMSN-E led to the consumption of intracellular GSH. Therefore, intracellular ROS levels in HREC were expected to be elevated by HMSN-E. To verify this hypothesis, DCFH-DA was used to detect the change of intracellular ROS levels. As shown in Figure 4D and E, the intracellular ROS levels in HREC were influenced by HMSN-E. After incubation of HREC with HMSN-E for 24 h, the intracellular ROS in HREC increased with an increase in HMSN-E concentration, indicating that HMSN-E could induce the elevation of intracellular ROS in HREC.

The generation of H_2S at high concentrations in tumor cells has been explored as a potential method for cancer treatment. Many H_2S donors, including H_2S-generator nanocarriers, have been proven to have antitumor effects via the induction of acidosis, blockade of survival pathways, and disturbance of cell cycles.[62,71,72] H_2S has been reported to disrupt normal mitochondrial function, and its donors can reduce mitochondrial membrane potential (MMP).[73,74] To investigate the influence of HMSN-E on mitochondrial function in HREC, MMP changes were analyzed by flow cytometry using JC-1 probes. The JC-1 probe emits red fluorescence in normal mitochondria with high MMP and converts to green fluorescence when the MMP decreases. A decrease in MMP can be easily observed by detecting the transition of JC-1 from red to green. As shown in Figure 5A–D, HMSN-E clearly changed the fluorescence of JC-1 compared with that in the control groups. An increase in the HMSN-E concentration led to a decrease in red fluorescence and an increase in green fluorescence. It could be inferred that HMSN-E decreased the MMP in HREC.

The cell cycle-mediating processes were also one of the targets for H_2S. Some H_2S donors can induce cell arrest at the G1/S, S-G2/M, and G2/M checkpoints in different cell types.[72] As shown in Figure 5E–H, the proportion of HREC in G1 increased as the HMSN-E concentration increased. Therefore, it could be inferred that HMSN-E, as a H_2S nanogenerator, could induce cell arrest at the G1/S checkpoint in HREC, which is in agreement with the effect of the H_2S donor GYY4137 on the cell cycle of HCC cells.[75]

Although there is a complicated interplay among elevated intracellular ROS, decreased cellular MMP, and arrested cell cycle, these three factors have been widely reported to induce cell apoptosis via intricate pathways.[76–78] As expected, HMSN-E remarkably affected the apoptosis and necrosis of HREC as compared with the control group (Figure 5I–L). After incubation of HREC with HMSN-E for 24 h, the proportion of apoptotic and necrotic cells increased from 15.09% to 31.80% when the HMSN-E concentration was increased from 12.5 to 50 μg/mL. It could be concluded that HMSN-E could obviously induce cell apoptosis and necrosis.

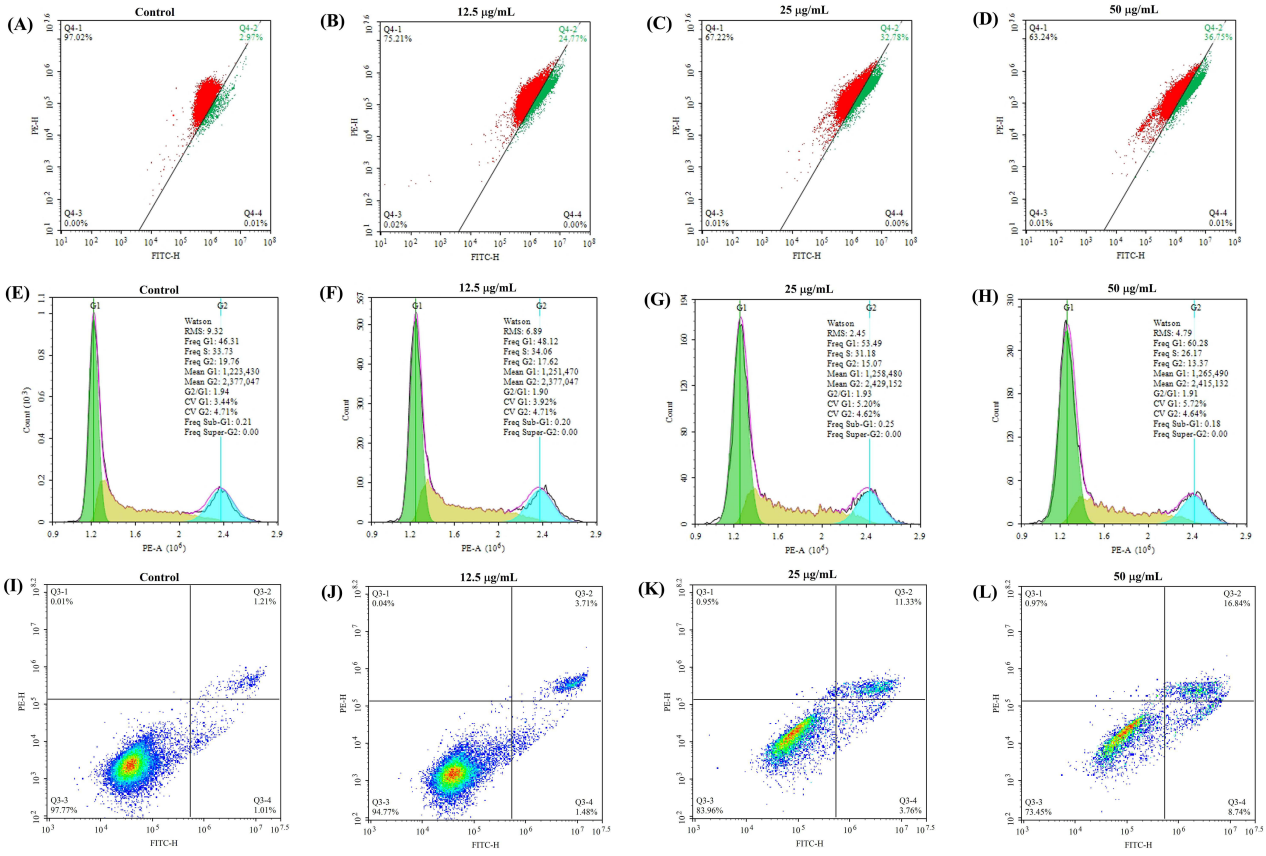

Figure 5 The mechanism for the toxic effect of HMSN-E on HREC analyzed by flow cytometric. (**A–D**) The influence of HMSN-E on the MMP of HREC. (**E–H**) the influence of HMSN-E on the cell cycle distribution of HREC. (**I–L**) the influence of HMSN-E on the cell apoptosis and necrosis for HREC.

Evaluation of the Ocular Toxicity of HMSN in vivo

For topical eye drops, HMSN-E dispersed in normal saline at different concentrations (50, 100, and 200 μg/mL) was dripped into the mouse ocular conjunctival sac qid for 2 weeks. After the cornea was stained with fluorescein, images of the mouse eyes were recorded using a slit-lamp microscope. As shown in Figure 6A, when the mice were treated with 50 μg/mL HMSN-E, the eyeball presented similar dye staining to the control group and showed nearly no green fluorescence, indicating that a low concentration of HMSN-E was safe for ocular corneal tissue. However, green fluorescence was observed when the HMSN-E concentration reached 100 μg/mL, and the fluorescence intensity increased with increasing HMSN-E concentration, which indicated that high concentrations of HMSN-E (≥100 μg/mL) could lead to corneal damage.

After the mice were treated via intravitreal injection with different concentrations of HMSN-E (5, 10, and 20 μg/mL), images of the eyes after mydriasis were recorded using a slit lamp microscope. As shown in Figure 6B, PBS treatment led to nearly no change compared with the control group. However, when the mice were treated with HMSN-E, the opacity of the mouse lenses gradually worsened as the concentration of HMSN-E increased, indicating that HMSN-E caused damage to the mouse lens, thereby causing cataracts.

To further investigate the effect of HMSN-E on eye tissues, eye tissues were collected and embedded in paraffin to prepare eyeball sections. The eyeball slices were stained with hematoxylin and eosin (H&E) to analyze the toxic effects of HMSN-E on retinal tissues. As shown in Figure 7A, the layers of the retina in the PBS-treated group and the control group were well-aligned and had clear boundaries, which suggested that intravitreal injection with PBS showed no effect on the mouse retina. In the HMSN-E-treated groups, the arrangement of mouse ganglion cells became increasingly irregular as the concentration of HMSN-E was increased. Abnormal vascular proliferation in the ganglion cell layers and retinal neovascularization induced by inflammation in the ganglion cell layer were observed in the groups treated with high concentrations of HMSN-E (10 and 20 μg/mL). Therefore, it can be inferred that ganglion cell layers were subjected to HMSN-E disturbance. However, the arrangement of cell layers in the inner plexiform layer, inner core layer, outer plexiform layer, and outer nuclear layer remained relatively regular in all groups, which indicated that these sections could not be affected by HMSN-E. Inflammation of the eyeball was evaluated by detecting tumor necrosis factor-α (TNF-α) expression using immunohistochemical staining. There was no obvious expression of TNF-α in the PBS group compared with that in the control group (Figure 7B). In the HMSN-E-treated groups, the expression of TNF-α in the vitreous cavity and retinal ganglion fiber layer increased as the concentration of HMSN-E increased.

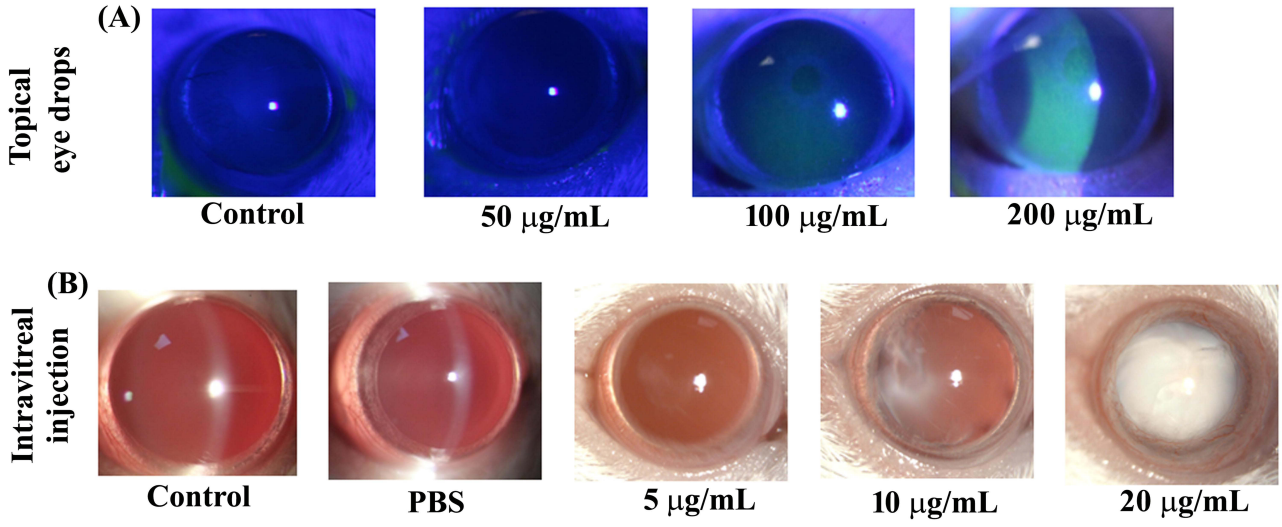

Figure 6 The effect of HMSN-E on eyeball tissue recorded via a slit lamp microscope. (**A**) the pictures of mouse eye corneas which were treated with HMSN-E (50, 100 and 200 μg/mL) and stained with fluorescein via topical eye drops recorded via a slit lamp microscope. (**B**) the pictures of mouse eyes which were treated with HMSN-E (PBS, 5, 10 and 20 μg/mL) via intravitreal injection recorded via a slit lamp microscope.

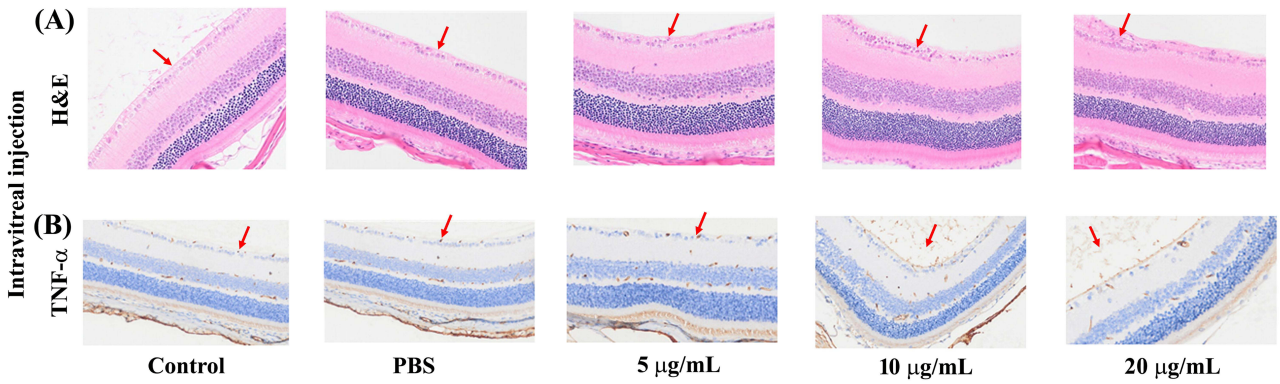

Figure 7 In vivo evaluation of ocular biosafety of HMSN-E. (**A**) H&E staining of retina tissue in each group (The red arrows pointing to the layers of retinal ganglion cells). (**B**) immunohistochemical staining of retina tissue in each group (The red arrows pointing to brown areas where TNF-α was immunohistochemically stained).

In the retina, the ganglion layers are closest to the vitreum as compared with other layers. Therefore, when HMSN-E was injected into the vitreum, the ganglion layers were most easily exposed to HMSN-E and subjected to HMSN-E-induced damage. As shown in the MTT assay, HMSN-E exerted cytotoxicity on HREC, which might induce inflammation in the ganglion cell layer, thereby resulting in abnormal vascular proliferation and retinal neovascularization.

As shown in the MTT assay, HMSNs caused obvious tetrasulfur content-dependent cytotoxic effects on the three selected cell lines. HCE-T, HLEC, and HREC originate from the cornea, lens, and retinal vessels, respectively, indicating that these tissues may also be influenced by HMSN-E. Therefore, a possible mechanism for the ocular toxicity induced by HMSN-E was proposed (Scheme 1). When HCE-T, HLEC, and HREC were treated with HMSN-E, intracellular GSH reacted with HMSN-E, resulting in the consumption of intracellular GSH and generation of H_2S, which might further lead to the elevation of intracellular ROS, decrease in cellular MMP, and cell cycle arrest at the G1/S checkpoint, subsequently inducing cell apoptosis and necrosis. Cell death of HCE-T, HLEC, and HREC may cause damage to the cornea, lens, and retinal vessels, respectively, such as corneal damage, lens opacity, and retinal abnormality.

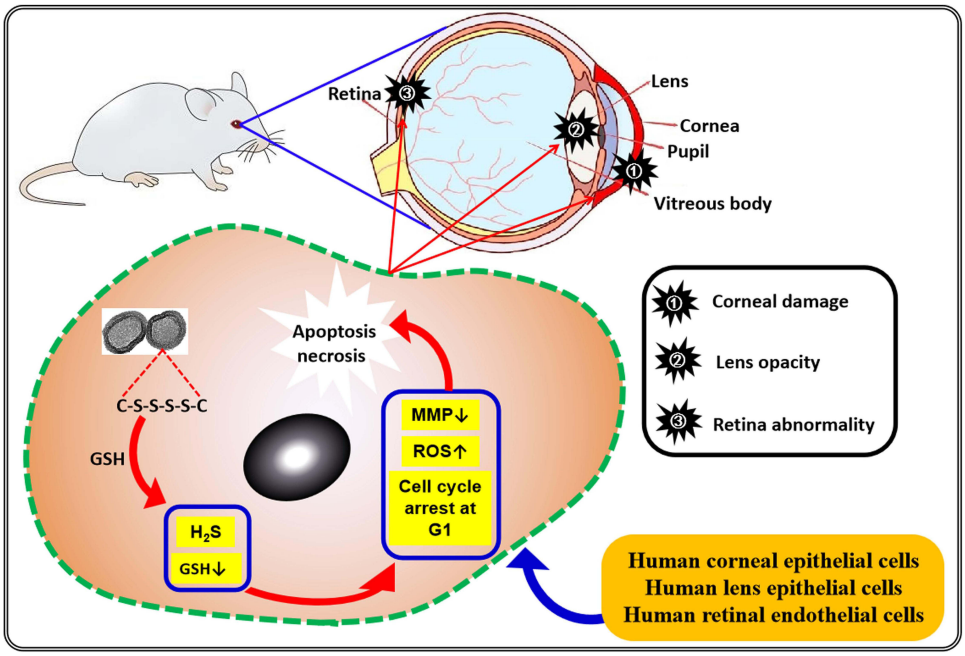

Scheme 1 A possible mechanism for HMSN-E-induced cytotoxicity.

Conclusion

In this study, HMSNs with different tetrasulfur bond contents were successfully prepared. Morphology, mesoporous pore size, BET surface area, and BET pore volume were all affected by the tetrasulfur bond content. The incorporation of tetrasulfur bonds made HMSNs vulnerable to GSH. The reaction of GSH with HMSNs containing tetrasulfur bonds could lead to the depletion of GSH and generation of H_2S. HMSNs caused obvious S-content-dependent cytotoxic effects on the three selected cell lines. HMSN-E, which had the highest tetrasulfur bond content, exhibited the highest cytotoxicity. HREC are most vulnerable to the toxicity of HMSNs. HMSN-E reacted with intracellular GSH to generate H_2S and decrease intracellular GSH concentrations. In addition, treatment of HREC with HMSN-E led to the elevation of intracellular ROS, a decrease in cellular MMP, and cell cycle arrest at the G1/S checkpoint, finally causing apoptosis and necrosis of HREC. The ocular biosafety of HMSN-E in vivo showed that topical eye drops of HMSN-E could lead to corneal damage and intravitreal injection of HMSN-E could induce inflammation in the vitreous and ganglion cell layers, thereby resulting in lens opacities and retinal abnormalities. In summary, the incorporation of tetrasulfur bonds into HMSN can have toxic effects on ocular tissues. Therefore, when mesoporous silica nanocarriers are designed for ophthalmic pharmaceuticals, the ocular toxicity of the tetrasulfur bonds should be considered. If the tetrasulfur bond is embedded into a drug delivery system as a synergistic therapeutic agent with other drugs to treat ocular tumors, it is necessary to improve the targeting ability of the carrier to avoid or reduce the toxic side effects.

Data Sharing Statement

All data generated or analyzed during this study are included in this publication.

Ethics Approval and Consent to Participate

All animal experiments were performed in accordance with the China Public Health Service Guide for the Care and Use of Laboratory Animals. Experiments involving mice and protocols were approved by the Institutional Animal Care and Use Committee of the Bengbu Medical University.

Author Contributions

All authors made a significant contribution to the work reported, whether that is in the conception, study design, execution, acquisition of data, analysis and interpretation, or in all these areas; took part in drafting, revising or critically reviewing the article; gave final approval of the version to be published; have agreed on the journal to which the article has been submitted; and agree to be accountable for all aspects of the work.

Funding

This work was financially supported by the Key Project of the Anhui Educational Committee (Grant No. 2022AH051419, KJ2021A0718, 2023AH051963), Bengbu Medical University Science and Technology Project (Grant No. 2023bypy013), and the Projects of the Anhui Science and Technology University for Talent Introduction (Grant No. SKYJ201801).

Disclosure

The authors declare that they have no conflicts of interest in this work.

References

1. Tian B, Bilsbury E, Doherty S, et al. Ocular drug delivery: advancements and innovations. *Pharmaceutics*. 2022;14(9):1931. doi:10.3390/pharmaceutics14091931
2. Urtti A. Challenges and obstacles of ocular pharmacokinetics and drug delivery. *Adv Drug Deliv Rev*. 2006;58(11):1131–1135. doi:10.1016/j.addr.2006.07.027
3. Kels BD, Grzybowski A, Grant-Kels JM. Human ocular anatomy. *Clin Dermatol*. 2015;33(2):140–146. doi:10.1016/j.clindermatol.2014.10.006
4. Brown L, Leck AK, Gichangi M, et al. The global incidence and diagnosis of fungal keratitis. *Lancet Infect Dis*. 2021;21(3):49–57. doi:10.1016/S1473-3099(20)30448-5
5. Stitt AW, Curtis TM, Chen M, et al. The progress in understanding and treatment of diabetic retinopathy. *Prog Retin Eye Res*. 2016;51:156–186. doi:10.1016/j.preteyeres.2015.08.001

6. Bartlett AH, Bartlett JD. Ophthalmic procedures for treatment of advanced ocular surface diseases. *Optom Vis Sci*. 2015;92(9):939–947. doi:10.1097/OPX.0000000000000659
7. Hazin R, Lum F, Daoud YJ. Ophthalmic features of systemic diseases. *Ann Med*. 2012;44(3):242–252. doi:10.3109/07853890.2011.572904
8. Awwad S, Mohamed Ahmed AHA, Sharma G, et al. Principles of pharmacology in the eye. *Br J Pharmacol*. 2017;174(23):4205–4223 doi:10.1111/bph.14024.
9. Ahmed S, Amin MM, Sayed S. Ocular Drug Delivery: a Comprehensive Review. *AAPS Pharm Sci Tech*. 2023;24(2):66. doi:10.1208/s12249-023-02516-9
10. Rodrigues FSC, Campos A, Martins J, et al. Emerging trends in nanomedicine for improving ocular drug delivery: light-responsive nanoparticles, mesoporous silica nanoparticles, and contact lenses. *ACS Biomater Sci Eng*. 2020;6(12):6587–6597. doi:10.1021/acsbiomaterials.0c01347
11. Nguyen DD, Lai JY. Advancing the stimuli response of polymer-based drug delivery systems for ocular disease treatment. *Polym Chem*. 2020;11(44):6988–7008. doi:10.1039/D0PY00919A
12. Luo LJ, Nguyen DD, Lai JY. Dually functional hollow ceria nanoparticle platform for intraocular drug delivery: a push beyond the limits of static and dynamic ocular barriers toward glaucoma therapy. *Biomaterials*. 2020;243:119961 doi:10.1016/j.biomaterials.2020.119961.
13. Jiang ZX, Liang K, Gao X, et al. Fe-curcumin nanozyme-mediated immunosuppression and anti-inflammation in experimental autoimmune uveitis. *Biomater Res*. 2023;27(1):131. doi:10.1186/s40824-023-00451-1
14. Gui SY, Tang WW, Huang ZH. Ultrasmall coordination polymer nanodots Fe-Quer nanozymes for preventing and delaying the development and progression of diabetic retinopathy. *Adv Funct Mater*. 2023;33(36):2300261. doi:10.1002/adfm.202300261
15. Luo LJ, Nguyen DD, Lai JY. Harnessing the tunable cavity of nanoceria for enhancing Y-27632-mediated alleviation of ocular hypertension. *Theranostics*. 2021;11(11):5447–5463. doi:10.7150/thno.54525
16. Nguyen DD, Luo LJ, Yang CJ, et al. Highly retina-permeating and long-acting resveratrol/metformin nanotherapeutics for enhanced treatment of macular degeneration. *ACS Nano*. 2023;17(1):168–183. doi:10.1021/acsnano.2c05824
17. Yang CJ, Nguyen DD, Lai JY. Poly(l-Histidine)-mediated on-demand therapeutic delivery of roughened ceria nanocages for treatment of chemical eye injury. *Adv Sci*. 2023;10(26):e2302174. doi:10.1002/advs.202302174
18. Yang CJ, Anand A, Huang CC, et al. Unveiling the power of gabapentin-loaded nanoceria with multiple therapeutic capabilities for the treatment of dry eye disease. *ACS Nano*. 2023;17(24):25118–25135. doi:10.1021/acsnano.3c07817
19. Bui HL, Su YH, Yang C-J, et al. Mucoadhesive, antioxidant, and lubricant catechol-functionalized poly(phosphobetaine) as biomaterial nanotherapeutics for treating ocular dryness. *J Nanobiotechnology*. 2024;22(1):160. doi:10.1186/s12951-024-02448-x
20. Ger TY, Yang CJ, Ghosh S, Lai J-Y. Biofunctionalization of nanoceria with sperminated hyaluronan enhances drug delivery performance for corneal alkali burn therapy. *Chem Eng J*. 2023;476:146864. doi:10.1016/j.cej.2023.146864
21. Nguyen DD, Lai JY. Synthesis, bioactive properties, and biomedical applications of intrinsically therapeutic nanoparticles for disease treatment. *Chem Eng J*. 2022;435(11):134970. doi:10.1016/j.cej.2022.134970
22. Cao F, Gui SY, Gao X, et al. Research progress of natural product-based nanomaterials for the treatment of inflammation-related diseases. *Mater Design*. 2022;218:110686. doi:10.1016/j.matdes.2022.110686
23. Wu KY, Tan K, Akbar D, et al. A new era in ocular therapeutics: advanced drug delivery systems for uveitis and neuro-ophthalmologic conditions. *Pharmaceutics*. 2023;15(7):1952. doi:10.3390/pharmaceutics15071952
24. Amrutkar CS, Patil SB. Nanocarriers for ocular drug delivery: recent advances and future opportunities. *Indian J Ophthalmol*. 2023;71(6):2355–2366. doi:10.4103/ijo.IJO_1893_22
25. Li SD, Chen LB, Fu Y. Nanotechnology-based ocular drug delivery systems: recent advances and future prospects. *J Nanobiotechnol*. 2023;21(1):232 doi:10.1186/s12951-023-01992-2.
26. Vallet-Regí M, Schüth F, Lozano D, et al. Engineering mesoporous silica nanoparticles for drug delivery: where are we after two decades? *Chem Soc Rev*. 2023;51(13):5365–5451 doi:10.1039/d1cs00659b.
27. Djayanti K, Maharjan P, Cho KH, et al. Mesoporous silica nanoparticles as a potential nanoplatform: therapeutic applications and considerations. *Int J Mol Sci*. 2023;24(7):6349. doi:10.3390/ijms24076349
28. Xu BL, Li SS, Shi R, et al. Multifunctional mesoporous silica nanoparticles for biomedical applications. *Signal Transduct Target Ther*. 2023;8(1):435. doi:10.1038/s41392-023-01654-7
29. Feng Y, Liao Z, Li MY, et al. Mesoporous silica nanoparticles-based nanoplatforms: basic construction, current state, and emerging applications in anticancer therapeutics. *Adv Healthc Mater*. 2023;12(16):2201884. doi:10.1002/adhm.202201884
30. Fan WP, Song MM, Li LP, et al. Endogenous dual stimuli-activated NO generation in the conventional outflow pathway for precision glaucoma therapy. *Biomaterials*. 2021;277:121074. doi:10.1016/j.biomaterials.2021.121074
31. Song MM, Li LP, Liu JM. Peroxynitrite-scavenging organosilica nanomedicines for light-controllable NO release and precision on-demand glaucoma therapy. *ACS nano*. 2023;17(21):20979–20990. doi:10.1021/acsnano.3c02685
32. Qu W, Meng B, Yu Y, et al. EpCAM antibody-conjugated mesoporous silica nanoparticles to enhance the anticancer efficacy of carboplatin in retinoblastoma. *Mater Sci Eng C*. 2017;76:646–651. doi:10.1016/j.msec.2017.03.036
33. Liao YT, Lee CH, Chen ST, et al. Gelatin-functionalized mesoporous silica nanoparticles with sustained release properties for intracameral pharmacotherapy of glaucoma. *J Mater Chem B*. 2017;5(34):7008–7013. doi:10.1039/C7TB01217A
34. Hu CC, Sun JG, Zhang Y, et al. Local delivery and sustained-release of nitric oxide donor loaded in mesoporous silica particles for efficient treatment of primary open-angle glaucoma. *Adv Healthc Mater*. 2018;7(23):1801047. doi:10.1002/adhm.201801047
35. Sun JG, Jiang Q, Zhang XP, et al. Mesoporous silica nanoparticles as a delivery system for improving antiangiogenic therapy. *Int J Nanomed*. 2019;14:1489–1501. doi:10.2147/IJN.S195504
36. Sun JQ, Nie HL, Pan PP, et al. Combined anti-angiogenic and anti-inflammatory nanoformulation for effective treatment of ocular vascular diseases. *Int J Nanomed*. 2023;18:437–453. doi:10.2147/IJN.S387428
37. Wu KY, Brister D, Bélanger P, et al. Exploring the potential of nanoporous materials for advancing ophthalmic treatments. *Int J Mol Sci*. 2023;24(21):15599. doi:10.3390/ijms242115599
38. Gisbert-Garzaran M, Manzano M, Vallet-Regi M. Mesoporous silica nanoparticles for the treatment of complex bone diseases: bone cancer, bone infection and osteoporosis. *Pharmaceutics*. 2020;12(1):83. doi:10.3390/pharmaceutics12010083

39. Lérida-Viso A, Estepa-Fernández A, García-Fernández A, et al. Biosafety of mesoporous silica nanoparticles; towards clinical translation. *Adv Drug Deliv Rev*. 2023;201:115049. doi:10.1016/j.addr.2023.115049
40. Rodríguez-Ramos A, Marín-Caba L, Iturrioz-Rodríguez N, et al. Design of polymeric and biocompatible delivery systems by dissolving mesoporous silica templates. *Int J Mol Sci*. 2020;21(24):9573. doi:10.3390/ijms21249573
41. Mohammadpour R, Yazdimamaghani M, Cheney DL, et al. Subchronic toxicity of silica nanoparticles as a function of size and porosity. *J Control Release*. 2019;304:216–232. doi:10.1016/j.jconrel.2019.04.041
42. Yang SA, Choi SM, Jeon SM, et al. Silica nanoparticle stability in biological media revisited. *Sci Rep*. 2019;8(1):185. doi:10.1038/s41598-017-18502-8
43. Hosseinpour S, Walsh LJ, Xu C. Biomedical application of mesoporous silica nanoparticles as delivery systems: a biological safety perspective. *J Mater Chem B*. 2020;8(43):9863–9876. doi:10.1039/D0TB01868F
44. Huang P, Qian XQ, Chen Y, et al. Metalloporphyrin-encapsulated biodegradable nanosystems for highly efficient magnetic resonance imaging-guided sonodynamic cancer therapy. *J Am Chem Soc*. 2017;139(3):1275–1284. doi:10.1021/jacs.6b11846
45. Huang P, Chen Y, Lin H, et al. Molecularly organic/inorganic hybrid hollow mesoporous organosilica nanocapsules with tumor-specific biodegradability and enhanced chemotherapeutic functionality. *Biomaterials*. 2017;125:23–37. doi:10.1016/j.biomaterials.2017.02.018
46. Zhang Q, Shen C, Zhao N, et al. Redox-responsive and Drug-Embedded Silica Nanoparticles With Unique Self-Destruction Features For Efficient Gene/Drug Codelivery. *Adv Funct Mater*. 2017;27(10):1606229. doi:10.1002/adfm.201606229
47. Li JL, Cheng YJ, Zhang C, et al. Dual drug delivery system based on biodegradable organosilica Core@Shell architectures. *ACS Appl Mater Interfaces*. 2018;10(6):5287–5295. doi:10.1021/acsami.7b17949
48. Fan WP, Lu N, Shen ZY, et al. Generic synthesis of small-sized hollow mesoporous organosilica nanoparticles for oxygen-independent X-ray-activated synergistic therapy. *Nat Commun*. 2019;10(1):1241. doi:10.1038/s41467-019-09158-1
49. Lu Y, Yang YN, Gu ZY, et al. Glutathione-depletion mesoporous organosilica nanoparticles as a self-adjuvant and Co-delivery platform for enhanced cancer immunotherapy. *Biomaterials*. 2018;175:82–92. doi:10.1016/j.biomaterials.2018.05.025
50. Moghaddam SPH, Yazdimamaghani M, Ghandehari H. Glutathione-sensitive hollow mesoporous silica nanoparticles for controlled drug delivery. *J Control Release*. 2018;282:62–75. doi:10.1016/j.jconrel.2018.04.032
51. Zhang LL, Wang LY, Yao HL, et al. Biodegradable and biocompatible monodispersed hollow mesoporous organosilica with large pores for delivering biomacromolecules. *J Mater Chem B*. 2017;5(39):8013–8025. doi:10.1039/C7TB01526G
52. Yang YN, Wan JJ, Niu YT, et al. Structure-dependent and glutathione-responsive biodegradable dendritic mesoporous organosilica nanoparticles for safe protein delivery. *Chem Mater*. 2016;28(24):9008–9016. doi:10.1021/acs.chemmater.6b03896
53. Wang KL, Li X, Wang HL, et al. Evaluation on redox-triggered degradation of thioether-bridged hybrid mesoporous organosilica nanoparticles. *Colloid Surf A*. 2021;608:125566. doi:10.1016/j.colsurfa.2020.125566
54. Sharma J, Polizos G. Hollow silica particles: recent progress and future perspectives. *Nanomaterials*. 2020;10(8):1599. doi:10.3390/nano10081599
55. Yang X, He DG, He XX, et al. Synthesis of hollow mesoporous silica nanorods with controllable aspect ratios for intracellular triggered drug release in cancer cells. *ACS Appl Mater Interfaces*. 2016;8(32):20558–20569. doi:10.1021/acsami.6b05065
56. Shi SX, Chen F, Cai WB. Biomedical applications of functionalized hollow mesoporous silica nanoparticles: focusing on molecular imaging. *Nanomedicine*. 2013;8(12):2027–2039. doi:10.2217/nnm.13.177
57. Li J, Xie LS, Li B, et al. Engineering a hydrogen-sulfide-based nanomodulator to normalize hyperactive photothermal immunogenicity for combination cancer therapy. *Adv Mater*. 2021;33(22):2008481. doi:10.1002/adma.202008481
58. Liu B, Liang S, Wang Z, et al. A tumor-microenvironment-responsive nanocomposite for hydrogen sulfide gas and trimodal-enhanced enzyme dynamic therapy. *Adv Mater*. 2021;33(30):2101223. doi:10.1002/adma.202101223
59. Yang ZB, Luo Y, Hu YN, et al. Photothermo-promoted nanocatalysis combined with H_2S-mediated respiration inhibition for efficient cancer therapy. *Adv Funct Mater*. 2021;31(8):2007991. doi:10.1002/adfm.202007991
60. Xu J, Zhu WC, Yao XX, et al. Mesoporous organosilica-based hydrogen sulfide nanogenerator for enhanced tumor chemotherapy. *ACS Appl Nano Mater*. 2023;6(13):12029–12039. doi:10.1021/acsanm.3c01824
61. Wang KY, Li Y, Wang X, et al. Gas therapy potentiates aggregation induced emission luminogen-based photoimmunotherapy of poorly immunogenic tumors through cGAS-STING pathway activation. *Nat Commun*. 2023;14(1):2950. doi:10.1038/s41467-023-38601-7
62. Li HN, Xu FX, Gao G, et al. Hydrogen sulfide and its donors: novel antitumor and antimetastatic therapies for triple-negative breast cancer. *Redox Biol*. 2020;34:101564. doi:10.1016/j.redox.2020.101564
63. Wang Y, Yang T, He Q. Strategies for engineering advanced nanomedicines for gas therapy of cancer. *Natl Sci Rev*. 2020;7(9):1485–1512. doi:10.1093/nsr/nwaa034
64. Chen F, Hong H, Shi SX, et al. Engineering of hollow mesoporous silica nanoparticles for remarkably enhanced tumor active targeting efficacy. *Sci Rep*. 2014;4:5080. doi:10.1038/srep05080
65. Fang XL, Chen C, Liu ZH, et al. A cationic surfactant assisted selective etching strategy to hollow mesoporous silica spheres. *Nanoscale*. 2011;3(4):1632–1639. doi:10.1039/c0nr00893a
66. Teng ZG, Wang CY, Tang YX, et al. Deformable hollow periodic mesoporous organosilica nanocapsules for significantly improved cellular uptake. *J Am Chem Soc*. 2018;140(4):1385–1393. doi:10.1021/jacs.7b10694
67. Teng SY, Han YD, Hu Y, et al. Swellable hollow periodic mesoporous organosilica capsules with ultrahigh loading capacity for hydrophobic drugs. *J Colloid Interf Sci*. 2023;630:266–273. doi:10.1016/j.jcis.2022.10.017
68. Chen Y, Xu PF, Chen HR, et al. Colloidal HPMO nanoparticles: silica-etching chemistry tailoring, topological transformation, and nano-biomedical applications. *Adv Mater*. 2013;25(22):3100–3105. doi:10.1002/adma.201204685
69. Cheng R, Feng F, Meng FH, et al. Glutathione-responsive nano-vehicles as a promising platform for targeted intracellular drug and gene delivery. *J Control Release*. 2011;152(1):2–12. doi:10.1016/j.jconrel.2011.01.030
70. Xiong YX, Xiao C, Li ZF, et al. Engineering nanomedicine for glutathione depletion-augmented cancer therapy. *Chem Soc Rev*. 2021;50(10):6013–6041. doi:10.1039/D0CS00718H
71. Cao X, Ding L, Xie Z, et al. A review of hydrogen sulfide synthesis, metabolism, and measurement: is modulation of hydrogen sulfide a novel therapeutic for cancer? *Antioxid Redox Signal*. 2019;31(1):1–38. doi:10.1089/ars.2017.7058

72. Ngowi EE, Afzal A, Sarfraz M, et al. Role of hydrogen sulfide donors in cancer development and progression. *Int J Biol Sci*. 2021;17(1):73–88. doi:10.7150/ijbs.47850
73. Li J, Li X, Yuan Y, et al. Efficient polysulfide-based nanotheranostics for triple-negative breast cancer: ratiometric photoacoustics monitored tumor microenvironment-initiated H_2S therapy. *Small*. 2020;16(39):2002939. doi:10.1002/smll.202002939
74. Fan XY, Fei WD, Zhang M, et al. Nanotherapeutics for hydrogen sulfide-involved treatment: an emerging approach for cancer therapy. *Nanotechnol Rev*. 2022;11(1):2320–2348. doi:10.1515/ntrev-2022-0130
75. Lu S, Gao Y, Huang XL, et al. GYY4137, a hydrogen sulfide (H(2)S) donor, shows potent anti-hepatocellular carcinoma activity through blocking the STAT3 pathway. *Int J Oncol*. 2014;44(4):1259–1267. doi:10.3892/ijo.2014.2305
76. Brillo V, Chieregato L, Leanza L, et al. Mitochondrial dynamics, ROS, and cell signaling: a blended overview. *Life*. 2021;11(4):332. doi:10.3390/life11040332
77. Zaib S, Hayyat A, Ali N, et al. Role of mitochondrial membrane potential and lactate dehydrogenase A in apoptosis. *Anticancer Agents Med Chem*. 2022;22(11):2048–2062. doi:10.2174/1871520621666211126090906
78. Sahoo BM, Banik BK, Borah P, et al. Reactive Oxygen Species (ROS): key components in cancer therapies. *Anticancer Agents Med Chem*. 2022;22(2):215–222. doi:10.2174/1871520621666210608095512